New Journal of Physics
The open access journal at the forefront of physics

Deutsche Physikalische Gesellschaft DPG
IOP Institute of Physics

Published in partnership with: Deutsche Physikalische Gesellschaft and the Institute of Physics

OPEN ACCESS

RECEIVED
4 May 2021

REVISED
2 September 2021

ACCEPTED FOR PUBLICATION
20 September 2021

PUBLISHED
12 October 2021

PAPER

Bio-inspired natural sunlight-pumped lasers

Francesco Mattiotti[1,2,3,4,*], **William M Brown**[5], **Nicola Piovella**[6,7], **Stefano Olivares**[6,7], **Erik M Gauger**[5] and **G. Luca Celardo**[8,9]

[1] ISIS (UMR 7006) and icFRC, University of Strasbourg and CNRS, 67000 Strasbourg, France
[2] Department of Physics, University of Notre Dame, Notre Dame, IN 46556, United States of America
[3] Dipartimento di Matematica e Fisica and Interdisciplinary Laboratories for Advanced Materials Physics, Università Cattolica, via Musei 41, Brescia I-25121, Italy
[4] Istituto Nazionale di Fisica Nucleare, Sezione di Pavia, via Bassi 6, Pavia I-27100, Italy
[5] SUPA, Institute of Photonics and Quantum Sciences, Heriot-Watt University, Edinburgh, EH14 4AS, United Kingdom
[6] Dipartimento di Fisica 'Aldo Pontremoli', Università degli Studi di Milano, via Celoria 16, Milano I-20133, Italy
[7] Istituto Nazionale di Fisica Nucleare, Sezione di Milano, via Celoria 16, Milano I-20133, Italy
[8] Benemérita Universidad Autónoma de Puebla, Apartado Postal J-48, Instituto de Física, 72570, Mexico
[9] Dipartimento di Fisica e Astronomia, Università di Firenze, Sesto Fiorentino 50019, Italy
[*] Author to whom any correspondence should be addressed.

E-mail: mattiotti@unistra.fr

Keywords: sunlight-pumped lasing, bio-inspired photonic devices, organic nanophotonics, novel lasing approaches, photosynthetic quantum technologies

Supplementary material for this article is available online

Abstract

Even though sunlight is by far the most abundant renewable energy source available to humanity, its dilute and variable nature has kept efficient ways to collect, store, and distribute this energy tantalisingly out of reach. Turning the incoherent energy supply provided by the Sun into a coherent laser beam would overcome several of the practical limitations inherent in using sunlight as a source of clean energy: laser beams travel nearly losslessly over large distances, and they are effective at driving chemical reactions which convert sunlight into chemical energy. Here we propose a bio-inspired blueprint for a novel type of laser with the aim of upgrading unconcentrated natural sunlight into a coherent laser beam. Our proposed design constitutes a novel and different path towards sunlight-pumped lasers. In order to achieve lasing with the extremely dilute power provided by natural sunlight, we here propose a laser medium comprised of molecular aggregates inspired by the architecture of natural photosynthetic complexes. Such complexes exhibit a very large internal efficiency in harvesting photons from a power source as dilute as natural sunlight. Specifically, we consider a hybrid structure, where photosynthetic complexes in purple bacteria (*Rhodobacter sphaeroides*) surround a suitably engineered molecular dimer composed of two strongly coupled chromophores. We show that if pumped by the surrounding photosynthetic complex, which efficiently collects and concentrates solar energy, the core dimer structure can reach population inversion, and reach the lasing threshold under natural sunlight. The design principles proposed here will also pave the way for developing other bio-inspired quantum devices.

1. Introduction

One of the most remarkable aspects of many natural molecular aggregates is their ability to efficiently process extremely weak sources of energy or signals for biological purposes. Examples of this include the ability of avian magneto-receptors to sense the extremely weak geomagnetic field [1–4], or the ability of aquatic bacterial photosynthetic systems to harvest sunlight in deep murky waters, where incident light levels are much reduced beyond the already dilute level on land [5, 6]. For instance, purple bacteria have the ability to exploit extremely weak light sources [5, 6] (less than 10 photons per molecule per second) and some species of green sulfur bacteria (GSB) even perform photosynthesis with geothermal radiation from

deep-sea hydrothermal vents at about 400°C [7]. A possible origin of this incredible ability of bacterial photosynthetic systems to utilise weak sources of incoherent light and funnel the collected energy to specific molecular aggregates, could be based on the high level of symmetry and hierarchical organization characterizing the antenna complexes of bacterial photosynthetic organisms. Nevertheless the role of symmetry in the efficiency of such systems is still under debate [5, 8, 9] and it is not essential to the proposal discussed in this manuscript, which is based only on the well-known efficiency of natural bacterial photosynthetic complexes. Photosynthetic antenna complexes [5, 6, 10–17] are comprised of a network of chlorophyll molecules which are typically modelled as two-level systems (2LS) capable of absorbing radiation and transporting the resulting electronic excitation to the reaction center (RC) where charge separation occurs, a process which precedes and drives all other photosynthetic steps. Each 2LS has an associated transition dipole moment (TDM) which determines its coupling with both the electromagnetic field and also with other proximal chlorophyll molecules. Owing to the low solar photon density, photosynthetic aggregates operate in the single-excitation regime, meaning at most one excitation is present in the system at any one time. Many molecular aggregates, both naturally occurring as well as artificially synthesized, display bright and dark states in their single-excitation manifold [18–21]: J-aggregates are characterized by a bright state below the energy of the monomer absorption peak, while H-aggregates are characterized by a bright state above the energy of the monomer absorption peak. Cooperative properties, such as those seen in photosynthetic aggregates, have inspired many proposals for engineering artificial light-harvesting devices [22–29]. Moreover, the lasing properties of molecular aggregates, such as organic crystals (3D molecular aggregates) which display strong cooperative effects in the form of H- or J-aggregates, have been widely investigated [30–32].

The design principles of natural photosynthetic complexes rely on several levels of organization. On the lower level, single molecular aggregates feature a high degree of symmetry which favours the formation of bright (superradiant) or dark (subradiant) states with, respectively, large or small dipole strength [5, 6, 15, 33]. On a higher level, photosynthetic systems assemble many of these symmetric aggregates into larger structures, characterized by a hierarchy of energy levels, to maximize lightharvesting and energy transport. For instance, in purple bacteria, symmetric rings of chlorophyll molecules (LHI and LHII) surround the RC. These rings are J-aggregates with superradiant bright states which favor the absorption of light and the transfer of the excitation between each other [5, 6].

In this article, inspired by the design of the photosynthetic apparatus of purple bacteria [5, 6], we show that bio-mimetic molecular aggregates hold the promise of significantly lowering the threshold requirements for sunlight-pumped lasers.

Sunlight is by far the most abundant renewable energy source on Earth (a single hour of sunlight provides all the energy humanity uses in a whole year). Despite this, there remain significant limitations in utilising sunlight as it is both dilute and variable. Therefore, efficient storage and distribution of energy harvested from sunlight is paramount. In this respect, sunlight-pumped lasing is an extremely promising technology for energy harvesting, distribution and storage of solar energy [34]. Sunlight-pumped lasers transform natural incoherent sunlight into intense beams of coherent light, which can be used to efficiently distribute the collected energy and drive chemical reactions as a way to efficiently store solar energy. Indeed, sunlight-pumped lasers have been proposed as essential elements in several renewable energy technologies such as the magnesium cycle [35–37].

Since the power density in natural sunlight is very dilute, typically concentrated sunlight is needed to cross the lasing threshold. Experimentally, a concentration of 10^5 'suns' (1 Sun $= 0.14$ W cm^{-2}) is reachable, but clearly the smaller the 'number of suns' required for reaching the lasing threshold the better, since this lowers cost, technical demand, and increases efficiency. The first sunlight-pumped laser was realized in 1963 [34] and most sunlight-pumped lasers operate above 1000 suns [38]. Typically, the concentration of sunlight relies on imaging or non-imaging concentrators. One of the most efficient way to concentrate sunlight is through black-body cavity pumping, where concentrated sunlight collected by a mirror heats a black-body cavity to temperatures which range from 1000 K to 3000 K [34]. Recently, sunlight-pumped lasing has been demonstrated under natural sunlight intensity [39]. In this groundbreaking experimental work, a dye solution and a dichroic mirror are used to boost the pumping of the solid-state gain medium: the dye solution absorbs sunlight but its emitted fluorescent light is trapped in the cavity due to the dichroic mirror; this effectively increases the pumping rate of the lasing medium. By contrast, we propose a fully organic architecture based on natural photosynthetic antenna complexes. Besides bio-compatibility and non-toxicity, this may potentially offer advantages for realising nanolasers, as well as broad scope for molecular engineering and tailoring of different antenna complexes.

Our proposed bio-inspired molecular architecture has at its core a suitably engineered molecular H-dimer. In an H-dimer the interaction between the excited states of each molecules creates a bright state at high energy and a dark state at low energy. Under illumination, energy is absorbed mainly by the bright

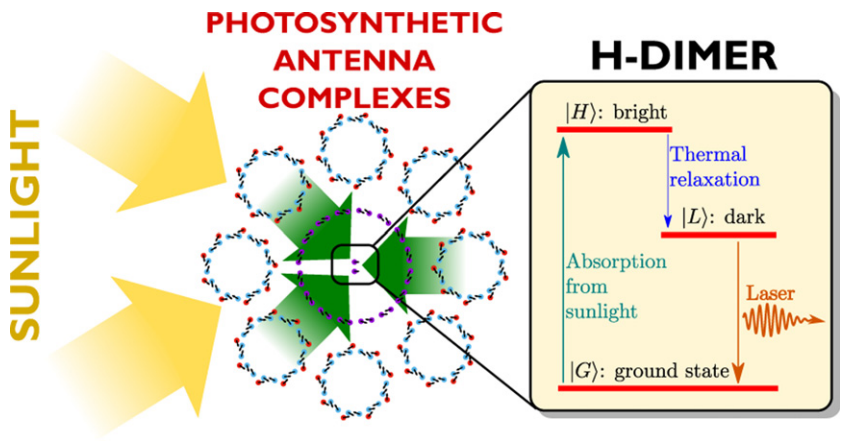

Figure 1. Pictorial representation of the design principle presented in the text. A photosynthetic antenna complex collects energy from sunlight, which is converted to an electronic excitation and efficiently funneled to an H-dimer placed in the middle. Here, the excitation is absorbed to a bright, high-energy state and it relaxes quickly to a dark, low-energy state. This mechanism prevents re-emission and allows population inversion between the $|L\rangle$ and $|G\rangle$ states and, therefore, lasing.

high-energy state and quickly transferred by thermal relaxation to the lower-energy state, which, being dark, loses energy by re-emission very slowly. Thus, an H-dimer is an ideal candidate to achieve population inversion (which is a main requirement for lasing) and its lower dark excitonic state can be exploited for the lasing transition. Nevertheless, natural sunlight is so weak that the required level of darkness of the lower excitonic state to achieve lasing would be unrealistically high. Indeed, the very long required excitonic lifetime of the lowest-excited state in the single-excitation manifold might be difficult to achieve in practice, due to disorder and competing nonradiative decay processes. In order to increase the pumping on the bright dimer state, so that the requirement on the darkness of the lower excitonic state can be relaxed, we consider surrounding a suitably engineered H-dimer by photosynthetic antenna complexes [5, 6], see figure 1. Indeed, natural antenna systems are extremely efficient precisely at collecting and funneling natural sunlight energy to specific locations. We show that a randomly positioned ensemble of such hybrid molecular aggregates inside a double-mirror cavity can lase under natural (unconcentrated) sunlight for realistic dimer parameters.

2. Lasing equations for molecular aggregates

We derived lasing equations for a generic ensemble of molecular aggregates, see details in the supplementary material (SM) (https://stacks.iop.org/NJP/23/103015/mmedia), each made of N identical molecules, that are placed in an optical lasing cavity with suitably chosen frequency. The Hamiltonian of the molecular aggregate is written with the usual Pauli operators as

$$\hat{H}_{\rm S} = \sum_{j=1}^{N} \frac{\hbar\omega_{\rm A}}{2}\hat{\sigma}_j^z + \sum_{i,j}\Omega_{i,j}\left(\hat{\sigma}_i^+\hat{\sigma}_j^- + \hat{\sigma}_j^+\hat{\sigma}_i^-\right), \tag{1a}$$

$$where \Omega_{i,j} = \frac{\vec{\mu}_i\cdot\vec{\mu}_j}{r_{ij}^3} - 3\frac{(\vec{\mu}_i\cdot\vec{r}_{ij})(\vec{\mu}_j\cdot\vec{r}_{ij})}{r_{ij}^5} \tag{1b}$$

is the dipolar inter-molecular coupling [15, 33, 40] with $\vec{\mu}_j$ being the TDM of the jth molecule in the aggregate and $\vec{r}_{ij}$ the vector between the ith and the jth molecule[10]. Equation (1a) and (1b) represents a molecular aggregate where each molecule is approximated as a 2LS with splitting $\omega_{\rm A}$. Under the relatively weak pumping conditions considered here, rather than retaining the full Hilbert space of dimension 2^N it suffices to limit our analysis to the overall aggregate ground state $|G\rangle$ and the single-excitation manifold comprised of N states $|j\rangle$ where the jth molecule is excited while all the other ones are in their respective ground states.

We capture thermal relaxation by coupling each molecule to an independent bath of harmonic oscillators [26, 29], and for simplicity we here neglect vibronic effects [21]. The interaction of molecular

[10] Closely spaced molecules require a modification of the dipole interaction term which is then not solely determined by the TDM [10, 11].

aggregates with solar radiation has been widely discussed in the literature [23, 24, 41–48]. Here, we consider the well-established Bloch–Redfield (BR) formalism for the interaction with a black-body radiation at the temperature of the Sun, which also underpins the recent work in references [23, 24, 42]. As the BR master equation has not been secularised, coherence and population dynamics are not decoupled, however, as we will later only be interested in the effective optical pumping rate, we do not expect subtleties regarding the absorption process and transient coherences [42] to be important. Within this framework, the interaction of the molecular aggregates with the phonon and photon bath is then governed by the master equation

$$\frac{\mathrm{d}\hat{\rho}(t)}{\mathrm{d}t} = -\frac{\mathrm{i}}{\hbar}\left[\hat{H}_{\mathrm{S}}, \hat{\rho}(t)\right] + \mathcal{D}_{\mathrm{BB}}[\hat{\rho}(t)] + \mathcal{D}_{\mathrm{T}}[\hat{\rho}(t)], \tag{2}$$

where $\mathcal{D}_{\mathrm{BB}}$ and $\mathcal{D}_{\mathrm{T}}$ are the BR dissipators for the coupling to the black-body cavity and phonon environments, respectively (see SM). In our simulations phonon bath parameters have been chosen in order to effect thermal relaxation within a few picoseconds, typical of molecular aggregates [5, 6]. Equation (2) can be largely simplified under well-motivated assumptions: first, as we check and validate numerically in the SM, for the parameter regimes of interest we may safely secularise and reduce our master equation to Lindblad form [49]; this is consistent with the approach of the recent works [41, 46]. In deriving the laser equation, we shall make a further assumption, which is analyzed in detail and validated by numerical simulations in the SM: since thermal relaxation is typically the fastest time scale for molecular aggregates at room temperature (RT), we can assume that the populations in the single-excitation manifold are always at thermal equilibrium.

Using the above mentioned assumptions, the coupling with the black-body photon bath is well-approximated by rate equations for the populations (see SM and reference [46]), with absorption rates between the $|G\rangle$ and the single-excitation states $|k\rangle$ given by

$$R_k = n_{\mathrm{T}}^k \gamma_k, \quad \text{with } \gamma_k = \frac{\mu_k^2 \omega_k^3}{3\pi\epsilon_0 \hbar c^3} \quad \text{and} \quad n_{\mathrm{T}}^k = \frac{1}{\mathrm{e}^{E_k/k_{\mathrm{B}}T_{\mathrm{BB}}} - 1}, \tag{3}$$

where γ_k is the spontaneous decay rate of the kth state, ω_k and μ_k its transition frequency and TDM, respectively, $E_k = \hbar\omega_k$ the transition energy and n_{T}^k the photon occupancy at the black-body temperature T_{BB}.

As our laser gain medium, we consider an ensemble of molecular aggregates randomly distributed with density n_{A} inside a lasing cavity of frequency ω_{c} and containing a classical oscillating field $\vec{E} = E_0\hat{\epsilon}\,\cos(\omega_{\mathrm{c}}t)$. The aggregate's single-excitation states $|k\rangle$ couple coherently to the cavity mode with Rabi frequencies $\Omega_k = (\vec{\mu}_k \cdot \hat{\epsilon})E_0/\hbar$ that depend on the cavity polarization $\hat{\epsilon}$ and field amplitude E_0. In molecular aggregates under weak pumping, the Rabi frequency is typically smaller than the interband excitonic dephasing rate, $\Gamma_\phi \gg \Omega_k$. Therefore, instead of coherent Rabi oscillations we obtain incoherent transition rates proportional to Ω_k^2, as derived in the SM and reference [50]. The field intensity $I = \epsilon_0|E_0|^2c/2$ can also be written as $I = \hbar\omega_{\mathrm{c}}nc/V$, where n is the number of photons in the cavity, V the cavity volume, and c the speed of light. This allows us to express the cavity-induced transition rate between $|G\rangle$ and $|k\rangle$ state in terms of the number of cavity photons n as

$$nB_k = n\frac{1}{3}\frac{|\mu_k|^2\omega_{\mathrm{c}}}{V\hbar\epsilon_0}\frac{\Gamma_\phi}{\Gamma_\phi^2 + (\Delta_k/\hbar)^2} = \frac{\Omega_k^2}{2}\frac{\Gamma_\phi}{\Gamma_\phi^2 + (\Delta_k/\hbar)^2}, \tag{4}$$

where $\Delta_k = (E_k - \hbar\omega_{\mathrm{c}})$ is the energy detuning between the single-excitation state k and the cavity mode. The factor $1/3$ derives from averaging over the random aggregate orientations.

Under the above assumption we can write lasing rate equations that couple the populations of the molecular aggregates with the number of photons in the cavity. For this purpose, let us define the density of aggregates in the excited states as $N_{\mathrm{e}} = n_{\mathrm{A}}P_{\mathrm{e}}$, the density of aggregates in the ground state as $N_{\mathrm{G}} = n_{\mathrm{A}}P_{\mathrm{G}}$, and the population difference per unit volume as $D = N_{\mathrm{e}} - N_{\mathrm{G}}$. This gives the lasing equations

$$\begin{aligned}\frac{\mathrm{d}D}{\mathrm{d}t} &= -D[R_d + R_u + (B_{\mathrm{tot}} + \langle B\rangle)n] + n_{\mathrm{A}}[R_u - R_d + n(B_{\mathrm{tot}} - \langle B\rangle)]\\ \frac{\mathrm{d}n}{\mathrm{d}t} &= V(B_{\mathrm{tot}} + \langle B\rangle)\frac{nD}{2} - V(B_{\mathrm{tot}} - \langle B\rangle)\frac{nn_{\mathrm{A}}}{2} - \kappa n,\end{aligned} \tag{5}$$

where $R_u = \sum_k R_k$ is the total absorption rate and $R_d = \sum_k (R_k + \gamma_k)p_k$ is the spontaneous and stimulated emission rate from the single-excitation manifold. Further, $B_{\mathrm{tot}} = \sum_k B_k$ and $\langle B\rangle = \sum_k B_k p_k$ are, respectively, the total upwards and downwards transition rates between $|G\rangle$ and the single-excitation manifold that are induced by the coupling to the cavity mode.

From equation (5) we obtain the stationary values of the population difference per unit volume D_0 and the stationary number of photons n_0 in the cavity

$$\begin{aligned} D_0 &= \frac{2\kappa}{V(B_{\text{tot}} + \langle B\rangle)} + n_{\text{A}}\bar{B}, \\ n_0 &= \frac{V(n_{\text{A}}D_{\text{eq}} - D_0)}{2\kappa}(R_u + R_d), \end{aligned} \tag{6}$$

where $\bar{B} = \left(B_{\text{tot}} - \langle B\rangle\right) / \left(B_{\text{tot}} + \langle B\rangle\right)$ and $D_{\text{eq}} = (R_u - R_d)/(R_u + R_d)$ is the equilibrium population difference in absence of driving from the cavity. Above the lasing threshold, i.e. having $n_0 > 0$ stationary photons in the cavity, the laser intensity and output power will be, respectively,

$$\begin{aligned} I &= \frac{\hbar\omega_{\text{c}}c}{V}n_0, \\ P_{\text{out}} &= \frac{\kappa V}{c}I = \kappa\hbar\omega_{\text{c}}n_0. \end{aligned} \tag{7}$$

We turn to the question under which conditions we achieve lasing. Imposing $n_0 > 0$ in equation (6) we require $n_{\text{A}}D_{\text{eq}} - D_0 > 0$, which can be written as

$$n_{\text{A}}(D_{\text{eq}} - \bar{B}) > \frac{2\kappa}{V(B_{\text{tot}} + \langle B\rangle)}\ . \tag{8}$$

Using the definitions of R_u and R_d and for $n_{\text{T}}^k \ll 1$,

$$D_{\text{eq}} \approx \frac{\sum_k \chi_k n_{\text{T}}^k - \langle\chi\rangle}{\sum_k \chi_k n_{\text{T}}^k + \langle\chi\rangle}, \quad \text{with } \langle\chi\rangle = \sum \chi_k p_k, \tag{9}$$

where $\chi_k = \gamma_k/\gamma_0$ indicates the relative brightness of the state $|k\rangle$ and $\langle\chi\rangle$ is the thermal average of the relative decay rates of all the single-excitation states. Moreover, $\gamma_0 = (\mu^2\omega_{\text{A}}^3)/(3\pi\epsilon_0\hbar c^3)$ is the spontaneous decay rate of a single molecule. We reiterate that equation (9) is generically valid subject to fast thermal relaxation and with negligible occupation of states containing more than one excitation. Both assumptions are realistic for molecular aggregates under black-body radiation pumping.

Equation (8) determines the critical density of molecular aggregates to achieve lasing, implying

$$D_{\text{eq}} > \bar{B}. \tag{10}$$

Since $\bar{B} \geqslant 0$ by definition, unsurprisingly we require population inversion, $D_{\text{eq}} > 0$, to achieve lasing. Considering equation (10) with equation (9) and recalling that $R_u = \gamma_0\sum_k \chi_k n_{\text{T}}^k$, implies $\langle\chi\rangle \leqslant \frac{R_u}{\gamma_0}\frac{1-\bar{B}}{1+\bar{B}}$, which can be recast as:

$$\langle\chi\rangle \leqslant \frac{R_u}{\gamma_0}\frac{\langle B\rangle}{B_{\text{tot}}}. \tag{11}$$

Equation (11) clearly shows that given a non-zero (but realistically small) value for $\langle\chi\rangle$, two conditions need to be met for lasing: (i) the ratio $\langle B\rangle/B_{\text{tot}}$ should be as large as possible, given $\langle B\rangle \leqslant B_{\text{tot}}$ this is maximized for $\langle B\rangle \approx B_{\text{tot}}$. This condition can be realised by a lasing state that is well-gapped (w.r.t. $k_{\text{B}}T$ at RT) below all other states in its excitation manifold; (ii) the absorption rate R_u should be as large as possible. Lasing under very weak pumping requires a highly dark aggregate (i.e. small $\langle\chi\rangle$), even if $\langle B\rangle \approx B_{\text{tot}}$. This is not easy to achieve, and the situation is compounded by nonradiative losses typically present in molecular aggregates. As we shall show in the following, a bio-inspired molecular architecture can help to mitigate this stringent demand and make lasing achievable.

Throughout this article, when considering black-body optical pumping, we choose a temperature $T_{\text{BB}} = 3000$ K which is attainable using sunlight concentrated by a mirror of a few m^2 [34] with an input power into the black-body cavity of few kW. To compute the laser output power we assume a typical gain medium volume of $V = 11.3$ cm^3 (radius of 6 mm and length of 10 cm). The densities of the laser medium are chosen to be lower than 1 aggregate/(10 nm)^3, corresponding to realistic densities for dye lasers: $n_{\text{A}}^{(\max)} = 10^{18}$ cm^{-3} $= 1.6$ mmol l^{-1} [51]. This choice ensures that direct interactions between the molecular aggregates can be neglected. Moreover, it also keeps the output power below 1 kW, so that thermal balancing with the black-body cavity under realistic sunlight pumping can be maintained. To remove the need for and complexity of sunlight concentration we shall also consider the possibility to achieve lasing under direct natural sunlight illumination. To model natural sunlight we consider pumping under a

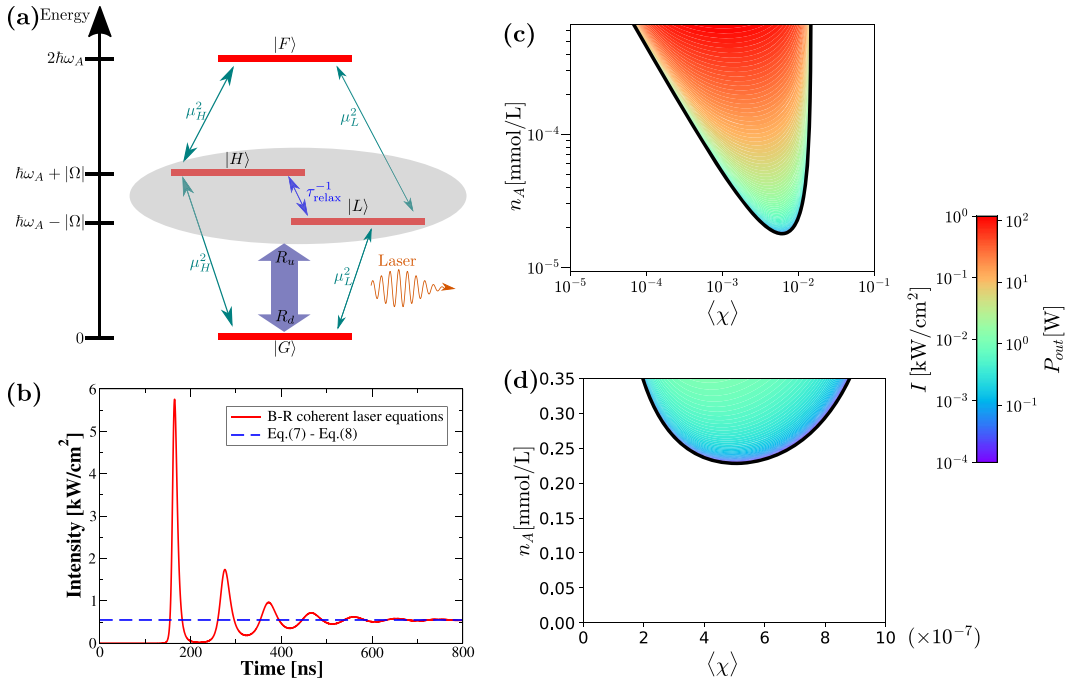

Figure 2. (a) Eigenstates of the dimer Hamiltonian $\hat{H}_S$ (equation (1a) and (1b)) and transition rates between them. Optical rates (green arrows) are proportional to the squared dipole strengths (see equation (3)), while the thermal relaxation rate (blue arrow) is $\tau_{\rm relax}^{-1} \approx 1\ {\rm ps}^{-1}$. All these transitions obey detailed balance, i.e. upwards and downwards rates are proportional to the Bose–Einstein occupation number $n_T(\hbar\omega)$ and $[1 + n_T(\hbar\omega)]$, respectively. The thick double arrow represents the resulting effective rates linking the ground state $|G\rangle$ to the single-excitation manifold (grayed area), as utilised in equation (5). The $|L\rangle$–$|G\rangle$ transition is further coupled to a resonant lasing cavity. (b) Temporal evolution of the laser intensity under black-body pumping: BR model (solid red) for dimers that are coherently coupled to the lasing cavity (details in the SM), and steady-state solution (dashed blue) of our lasing equations, equations (6) and (7). Parameters: $\mu = 10.157$ D, $\hbar\omega_A = 1.17$ eV, $\Omega = 2000\ {\rm cm}^{-1}$, $T_{BB} = 3000$ K, $\Gamma_\phi = 1/(10\ {\rm ps})$, $\kappa/(2\pi) = 50$ MHz, $\langle\chi\rangle = 0.005$, $n_A = 5 \times 10^{-4}$ mmol l^{-1}, and a lasing cavity volume $V = 11.3$ cm^3 (cylindrical shape of radius $R = 6$ mm and length $L = 10$ cm). (c) and (d) Laser intensity and output power for the same parameters as (b) except for $\langle\chi\rangle$ (thermal average of the relative brightness of single-excitation states with respect to a single molecule) and n_A (dimer density in millimole l^{-1}) which are varied along the axes. The black line represents the lasing threshold (equation (8)). In (c) optical pumping occurs via a black body radiation at $T_{BB} = 3000$ K, whereas in (d) the lasing medium is illuminated by natural sunlight.

black-body at $T_{BB} \approx 5800$ K but with rates in equation (3) reduced by a factor f_S representing the solid angle of the Sun as seen on Earth [52],

$$f_S = \frac{\pi r_S^2}{4\pi R_{ES}^2} = 5.4 \times 10^{-6}, \tag{12}$$

with r_S being the radius of the Sun and R_{ES} the Sun-to-Earth distance. In this case we limit the output power to 1 W since the incident power on our chosen lasing cavity is just a few W.

3. Lasing with dimers

Let us consider a dimer comprising two identical chromophores. Each molecule (labeled $j = 1, 2$) has one relevant optical transition, so that we may model it as a 2LS with ground state $|g_j\rangle$ and excited state $|e_j\rangle$. Excitation energy $\hbar\omega_A$ and magnitude μ of the electric TDM are identical between the molecules, while the direction of the optical dipole $\vec{\mu}_j$ depends on the orientation of its chromophores and may differ.

For this dimer system the Hamiltonian in equation (1a) and (1b) is diagonalized by a set of four states (see figure 2(a)): $|G\rangle = |g_1\rangle|g_2\rangle$, where both molecules are in their respective ground state; $|L\rangle$ and $|H\rangle$ are the lowest and highest single-excitation states, where only one excitation is present in the system, delocalised over both molecules; these states span the single-excitation manifold and they correspond to the symmetric and anti-symmetric states $\left(|g_1\rangle|e_2\rangle \pm |e_1\rangle|g_2\rangle\right)/\sqrt{2}$. Finally, $|F\rangle = |e_1\rangle|e_2\rangle$ has both molecules in their respective excited state. The corresponding energies are shown in figure 2(a).

Optical transitions between the levels are determined by the relative orientation of the single molecules. We indicate the transition dipoles between the ground state $|G\rangle$ and the states $|L\rangle$ and $|H\rangle$ with $\vec{\mu}_L$ and $\vec{\mu}_H$, respectively, see figure 2(a). The conservation of total oscillator strength demands that $\mu_L^2 + \mu_H^2 = \mu_1^2 + \mu_2^2 = 2\ \mu^2$ and we have an H-dimer if $\mu_L <\ \mu$ while if $\mu_L >\ \mu$ we have a J-dimer. The

coupling Ω between molecules can either have a dipolar or a different origin, see SM. Typical H-dimers feature splittings between their bright and dark states of several k_BT, and the lower state may be many hundreds times less bright than the upper state [18–21]. Here, we consider a dimer with excitation energy in the near-infrared $\hbar\omega_A = 1.17$ eV ($\lambda \approx 1060$ nm), transition dipole of $\mu = 10.157$ D (as for the bacteriochlorophyll-a molecule) and a coupling $\Omega = 2000$ cm^{-1} as in similar H-dimers [53].

Under black-body illumination, primarily the bright state $|H\rangle$ undergoes excitation, followed by rapid thermal relaxation to the lower dark $|L\rangle$ state. The large energetic separation between $|H\rangle$ and $|L\rangle$ makes this relaxation one-way, preventing environmental re-excitation into $|H\rangle$. In SM we show that it is possible to achieve population inversion provided the absorption rate $|G\rangle \to |H\rangle$ dominates over the spontaneous emission rate $|L\rangle \to |G\rangle$. We proceed to couple the $|L\rangle \to |G\rangle$ transition to a resonant lasing cavity and evaluate the lasing performance of the system using the equations derived in the previous section. Figure 2(b) shows the resulting laser intensity: once the stationary regime has been reached, there is perfect agreement between the intensity predicted by equation (5) with our numerically obtained results from a coherent BR model. The latter, derived in equations (S37) and (S43) of the SM, treats both photon and phonon environments in the BR formalism, includes the doubly excited state, and—as its main assumption—treats the laser field semi-classically, but nonetheless coherently coupled to the aggregates similarly to references [54, 55]. In figure 2(c) we show the dependence of the laser intensity and power output on n_A and $\langle\chi\rangle$ based on realistic choices for all other parameters (see caption). The white area highlights the region below the laser threshold equation (8) (black continuous line), where the dimer density n_A is too low to permit lasing. As one can see, an intensity of up to 1 kW cm^{-2} can be reached with a very low dimer concentration.

To assess the possibility of lasing under direct natural sunlight illumination (i.e. without a black-body cavity heated by concentrated sunlight), we show the lasing threshold and output power for this scenario in figure 2(d). Clearly, lasing is still theoretically possible but only for very low values of $\langle\chi\rangle$. In practice, this is challenging due to the competition of nonradiative decay and other sources of noise in realistic situations. Nevertheless, as we show in the next section, the critical value of $\langle\chi\rangle$ increases by orders of magnitude if the dimer is placed inside a purple bacteria molecular aggregate. Finally, note that for lasing we require a small yet finite value of $\langle\chi\rangle$. In the case of a homodimer (where for parallel TDMs the $|L\rangle$ dimer state would be fully dark) this can either arise as a consequence of the relative orientation of the TDMs, or through the presence of structural or energetic disorder.

4. Bio-inspired lasers

Whilst lasing with a gain medium composed of suitable H-dimers is realistic under black-body cavity pumping, achieving the extremely high optical darkness (small $\langle\chi\rangle$) for direct sunlight-pumped operation is a tall order. According to equation (11) $\langle\chi\rangle$ is upper-bounded by the pumping rate in units of γ_0 (assuming a favourable ratio $\langle B\rangle/B_{tot} \approx 1$). Thus increasing the effective pumping rate reduces the stringency of required darkness. A possible way of increasing pumping is to surround the dimer by a molecular aggregate that is capable of efficiently absorbing photons and transferring the resulting energy excitations to the $|H\rangle$ dimer state. The aggregate should absorb at an energy larger than the $|H\rangle$ dimer state energy in order to preserve the gap which separates the dimer lasing state from other states, so that $\langle B\rangle/B_{tot} \approx 1$. Note that under this condition $\langle\chi\rangle$ of the whole aggregate can remain very close to $\langle\chi\rangle$ of the dimer alone.

In the following, in section 4.1 we consider a dimer surrounded by the photosynthetic antenna complex of purple bacteria that thrive in very low light intensity [5, 6, 8, 9, 57]. Moreover, in section 4.2 a GSB antenna complex is used to increase the pumping of the dimer $|H\rangle$ state even further.

4.1. Purple bacteria

Purple bacteria feature a hierarchical structure of symmetric molecular aggregates which absorb light and direct the collected energy to the specific molecular aggregate of the RC. The purple bacteria RC contains a bacteriochlorophyll (BChl) dimer called the special pair, and is surrounded by a light-harvesting system I (LHI) ring comprising 32 BChl molecules. The LHI ring is a J-aggregate with two superradiant states at 875 nm that are polarized in the ring plane and close to the lowest excitonic state. The LHI ring is surrounded by several LHII rings, each featuring the B850 ring, a J-aggregate composed of 18 BChl molecules with two superradiant states at 850 nm, and the B800 ring composed of 9 BChl molecules with main absorption peak at 800 nm. This hierarchical structure is able to absorb photons at different frequencies and guide the collected energy down an energetic funnel to the RC through a process dubbed supertransfer, resulting from the coupling between the LHII-LHI superradiant states and the LHI-RC aggregates [5, 6, 8, 9].

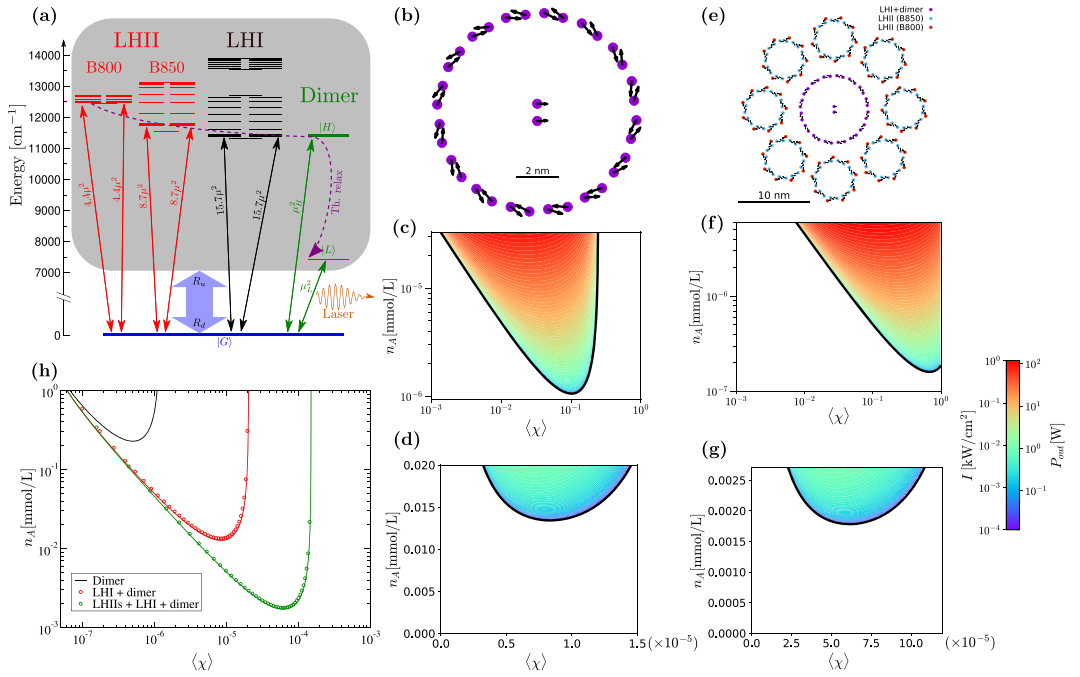

Figure 3. (a) Single-excitation eigenstates of the LHII complex (with a distinction between the B800 and the B850 subunits), LHI complex, and H-dimer. The strongest optical rates, proportional to the squared dipole strengths, are indicated alongside the two-headed arrows. As before, the thick double arrow represents the resulting effective rates linking the ground state $|G\rangle$ to the single-excitation manifold (grayed area) and the $|L\rangle$–$|G\rangle$ dimer transition is also coupled to a lasing cavity. The H-dimer parameters are: $\mu = 10.157$ D, $\hbar\omega_A = 1.17$ eV, $\Omega = 2000$ cm^{-1}. Further, $\Gamma_\phi = 1/(10\text{ ps})$, $\kappa/(2\pi) = 50$ MHz, and $V = 11.3$ cm^3. (b) and (e) Positions of the chromophores (circles) and transition dipole orientations (arrows) for the bio-mimetic complexes. Excitation energies and nearest-neighbour couplings for bio-mimetic aggregates are taken from references [8, 10, 11, 56, 57]. (c), (d), (f) and (g) Laser intensity and output power for an LHI ring surrounding an H-dimer ((c) and (d)) and with eight additional B800/850 LHII rings surrounding the LHI ring (f) and (g). On the axes we vary $\langle\chi\rangle$ of the H-dimer and n_A (the aggregate density in mmol l^{-1}). In all panels the black line represents the lasing threshold (equation (8)). In (c) and (f) we have black-body pumping at temperature $T_{BB} = 3000$ K, whereas (d) and (g) are for natural sunlight illumination. (h) Lasing threshold density under natural sunlight for a bare dimer, one LHI surrounding the dimer as in (b), and eight LHIIs around an LHI ring containing the dimer as in (e). The red and green continuous curves are for a dimer with a re-scaled R_u pumping rate: by a factor of 17 (red curve) and by a factor of 125 (green curve), corresponding to an enhancement factor $N/2$ with N being the number of chromophores in the aggregate. The circles are obtained from the full set of optical transitions as indicated in (a).

We here propose a hybrid structure, substituting the RC in the purple bacteria with an H-dimer whose $|H\rangle$ state is resonant with the superradiant states of LHI. Photons absorbed by the LHI ring would then contribute to the pumping of the dimer's $|H\rangle$ state, with the strong coupling between $|H\rangle$ and the bright state of the LHI complex ensuring fast transfer. The geometrical arrangement for this envisioned aggregate is shown in figure 3(b) [10, 11, 56, 57]. Specifically, at the centre of the LHI we place a homo-dimer with its two optical dipoles separated by 8 Å (similar to BChls in the special pair of purple bacteria RCs [5, 6]). We consider two transition dipoles that have an equal projection $\cos\theta$ onto the plane defined by the LHI ring, and opposite components $\pm\sin\theta$ orthogonal to the LHI plane. Controlling θ and keeping the coupling between the dimer molecules fixed, we can change the dimer brightness $\langle\chi\rangle$, so that we go from an H-dimer ($\theta \approx 0$, $\langle\chi\rangle \approx 0$) to a J-dimer ($\theta \approx \pi/2$, $\langle\chi\rangle \approx 1$). We chose the excitation frequency of the molecules in the dimer to be 1.17 eV corresponding to ≈ 1060 nm, which is in the near infrared wavelength. Since the coupling in the dimer is 2000 cm^{-1} the dimer $|H\rangle$ state has an excitation wavelength of about 875 nm at resonance with the superradiant states of the LHI aggregate. This choice ensures a large supertransfer coupling and fast thermal relaxation between the LHI and the dimer. Indeed due to the symmetric arrangement (the dimer is at the center of the LHI ring) the coupling between the $|H\rangle$ state of the dimer and the superradiant states of the LHI ring will be enhanced by a factor $\approx \sqrt{32}$ [5].

To model the purple bacteria antenna, we took the structure of LHI ring from reference [6, 57] and the structure of the LHII ring from reference [9]. The antenna complex molecular aggregates is described by the Hamiltonian in equation (1a) and (1b), where the nearest-neighbour couplings are replaced by the values reported in table 1. Other relevant model parameters are also reported in table 1, while the complete list of positions and dipole moments for each molecule can be found in the SM. We obtain the eigenvalues and the TDMs of all the energy states by direct Hamiltonian diagonalization, which allows evaluating the lasing equation (5) under the already discussed assumptions of negligible nonradiative losses and fast thermal relaxation. The latter is valid in this aggregate owing to supertransfer throughout the aggregate which

Table 1. Parameters for the aggregate Hamiltonian. The site energies are set to match the main fluorescence peaks at 800 nm (B800), 850 nm (B850) and 875 nm (LHI).

Subunit	Site energy (cm^{-1})	Nearest-neighbor coupling (cm^{-1})
LHII (B850)	12 532, 12 728 (alternate)	363, 320 (alternate) [9]
LHII (B800)	12 555	Dipole–dipole
LHI	12 911	806, 377 (alternate) [5, 6]
Dimer	9437	2000
Transition dipole	10.157 D [5, 6]	

entails thermal relaxation on the order of tens of picoseconds [10, 11]: this is much faster than optical pumping, which ranges from a few nanoseconds (large aggregates, high black-body temperature) down to milliseconds (small aggregates, natural sunlight) and spontaneous decay, of the order of a nanosecond for the brightest states. Moreover, other relevant timescales are the transition rate due to the coupling to the lasing cavity field which we estimate to be larger than hundreds of picoseconds (for the parameters considered here), and the realistic extraction rate κ from the cavity of about three nanoseconds which we considered. In summary, thermal relaxation is clearly the fastest process, justifying the use of equation (5) for analyzing the lasing response of such bio-inspired aggregates. Moreover, in the SM, results of incoherent laser equations, see equation (S60) in SM, which do not assume quasi-instantaneous thermalization, are shown to be in excellent agreement with equation (5).

The calculated lasing intensity and output power for a disordered ensemble of such aggregates (LHI + H-dimer) is shown in figure 3(c) for black-body cavity pumping, and in figure 3(d) for natural sunlight illumination. Comparing figures 2(c) and (d) with figures 3(c) and (d), the critical aggregate density to cross the lasing threshold is greatly lowered, and more importantly, the required level of the dimer darkness for the natural sunlight case is reduced by more than an order of magnitude. We obtain a further improvement when surrounding our LHI ring with eight LHII rings, see figure 3(e) (a magnified version of the figure can be seen in the SM, see figure S7). The B800/850 LHII aggregate level structure next to that of the LHI and H-dimer is shown in figure 3(a). As shown in figures 3(f) and (g) this larger aggregate architecture achieves a further lowering of the lasing threshold, i.e. increase of the critical value of $\langle\chi\rangle$ for the H-dimer below which lasing is possible. Interestingly, in figure 3(f), the addition of the rings has increased the effective pumping of the H-dimer to the extent where the dimer no longer has to feature a dark state to lase: indeed in this case lasing is possible even for $\langle\chi\rangle = 1$.

We have established that surrounding an H-dimer with purple bacteria LHI and LHII rings not only lowers the necessary threshold density but also enables lasing with much less dark H-dimers. To better understand and visualise these trends, we map out the lasing transition as a function of threshold density and average brightness of the H-dimer for natural sunlight pumping in figure 3(h).[11] This uses an H-dimer system described by equations (8) and (9) but with effective pumping R_u increased by the factor $N/2$, where N is the number of molecules in the bio-inspired aggregate including the H-dimer. This is a simplified approach of approximating enhanced pumping compared to the approach above based on the known TDMs of LHI/LHII states. Interestingly, the resulting threshold lines in figure 3(h) perfectly reproduce those obtained in the presence of the whole aggregate (symbols). This confirms that the crucial role of adding bio-inspired aggregates is to increase the effective pumping rate. Moreover, it suggests that our proposed architecture is scalable and an even lower lasing threshold could be achieved with larger J-aggregates surrounding the H-dimer, as we discuss in section 4.2, where we consider another bio-inspired architecture where the antenna complex of the GSB pumps the dimer $|H\rangle$ state. Nevertheless, caution is necessary when applying the lasing equations derived here to very large aggregates, where the assumption of thermalization occurring on the fastest relevant timescale can become invalid, in which case an incoherent laser equation might be more appropriate as discussed in the following.

The advantage of our proposed bio-inspired lasing medium over H-dimers can be also seen in terms of the amount of sunlight needed to reach the lasing threshold for a given dimer darkness. To illustrate this point, in figure 4 we show the output laser power as a function of the sunlight concentration, that is determined by the factor f_S: the value in equation (12) represents a concentration of '1 Sun', while we re-scale $f_S \to x f_S$ to reproduce 'x suns'. The density of molecules in the cavity is kept fixed, $N n_A = 0.7$ mmol l^{-1}, where N is the number of molecules per aggregate, while n_A is the aggregate density. The latter has to change with the number of molecules if we want to keep $N n_A$ fixed. Indeed, the dimer counts as two molecules, LHI ring contains 32 molecules and each LHII ring contains $18 + 9 = 27$

[11] The case of a black body pumping at $T_{BB} = 3000$ K is discussed in the SM.

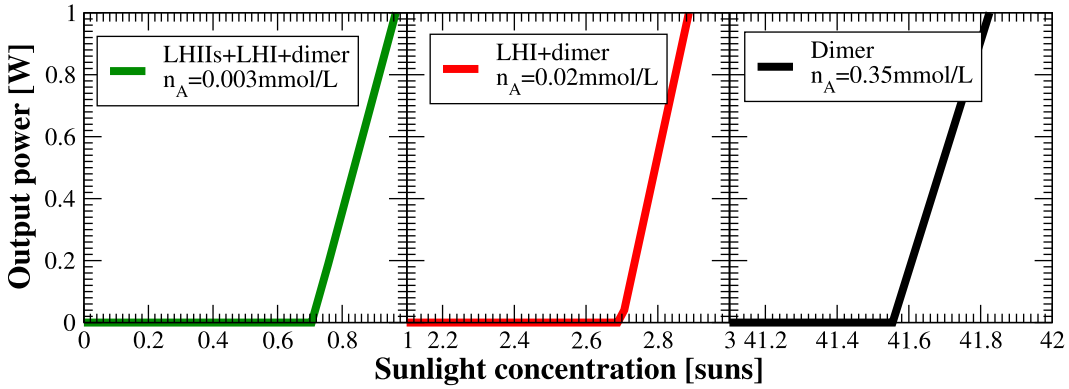

Figure 4. Output laser power, see equation (7), as a function of the sunlight concentration. Each panel refers to a different configuration, see figure. The sunlight concentration is changed by varying the factor f_S, where the value in equation (12) represents '1 Sun' in this figure. The dimer brightness is $\langle\chi\rangle = 5 \times 10^{-5}$ in all panels, while the aggregate density n_A is changed in order to keep the same density of molecules, $Nn_A \approx 0.7$ mmol l^{-1} (here N is the number of molecules per aggregate: $N = 2$ for the dimer, $N = 34$ for the LHI + dimer and $N = 250$ for the antenna complex + dimer). Other parameters: $\mu = 10.157$ D, $\hbar\omega_A = 1.17$ eV, $\Omega = 2000$ cm^{-1}, $\Gamma_\phi = 1/(10\text{ ps})$, $\kappa/(2\pi) = 50$ MHz, and $V = 11.3$ cm^3.

molecules. The dimer brightness is also kept fixed at $\langle\chi\rangle = 5 \times 10^{-5}$: at this value, lasing under natural sunlight ('1 Sun') is possible only for the full purple bacteria antenna complex (compare figure 3(g) with figures 2(d) and 3(d)). Here, figure 4 shows that a minimal sunlight concentration is needed to reach the lasing threshold, confirming the advantage of our proposed lasing medium: in fact, while for the isolated dimer a sunlight concentration of more than 41 suns is needed (see figure 4, right panel), this requirement drops to ≈ 2.7 suns if each dimer is surrounded by a single LHI ring (central panel), and to less than 1 Sun when the full purple bacteria antenna complex surrounds the dimer (left panel).

4.2. Green sulfur bacteria

While in the previous subsection we considered a bio-inspired aggregate which mimics the architecture of purple bacteria antennae, here we consider a different bio-inspired aggregate which mimics the architecture of another natural photosynthetic complex: the GSB antenna complex [58]. We are motivated in doing so since, as we pointed out above, the lasing efficiency of the bio-inspired aggregate increases with the number of molecules composing the aggregate; the GSB antenna photosynthetic complex is the largest and most efficient antenna complex present in nature [58]. Indeed, GSB antenna complexes can contain up to 250 000 BChl molecules. Even if the precise structure of the GSB antenna complex is not fully known and it can vary a lot in natural samples, one of the most important molecular structures present in GSB antennae are certainly constituted by self-aggregated BChl-c nanotubular structures [33]. Typically in GSB an ensemble of molecular structures (molecular nanotubes and lamellae) absorb sunlight and transfer excitation to a two-dimensional aggregate called the 'baseplate', which lies below the nanotubular structures. FMO complexes, which transfer excitations from antennae to reaction centres are attached to the baseplate.

Here we propose to enhance the pumping of the dimer $|H\rangle$ state by placing a natural nanotubular BChl-c aggregate close to the H-dimer as shown in figure 5(a), where the positions and TDM orientations of the molecules composing the nanotubular structures and the dimers are shown. The nanotube structure is described in [33] and references therein. The nanotube is composed by BChl-c molecules which have an excitation energy of 1.9 eV and a TDM of $\sqrt{30}$ D. The coupling between the BChl molecules in the nanotube produces a superradiant excitonic state state around 750 nm [33]. As for the dimer, we place it 3 nm from the wall of the nanotube (the same distance of the baseplate). The excitation frequency of the molecules composing the dimer (1.4 eV) and their coupling 2000 cm^{-1} are chosen so that the dimer $|H\rangle$ state is close in energy to the superradiant state of the nanotube. This configuration is considered here as an example of how increasing the number of chromophores in the antenna could enhance the lasing efficiency. In the future more sophisticated configurations, such as adding a baseplate and substituting the RC connected to the baseplate with H-dimers, could be analyzed.

As was done for the purple bacteria, we diagonalize the appropriate Hamiltonian, as reported in reference [33], to obtain the eigenvalues and the TDM of the eigenstates of the whole aggregate and we then use equation (8) to obtain the threshold density of lasing as a function of the brightness $\langle\chi\rangle$ of the dimer under natural sunlight pumping. The results are shown in figure 5(b), where symbols refer to the threshold density obtained from equation (8). The threshold density is shown for different nanotube lengths which contain different number of molecules N, see figure 5. The continuous lines represent the density threshold

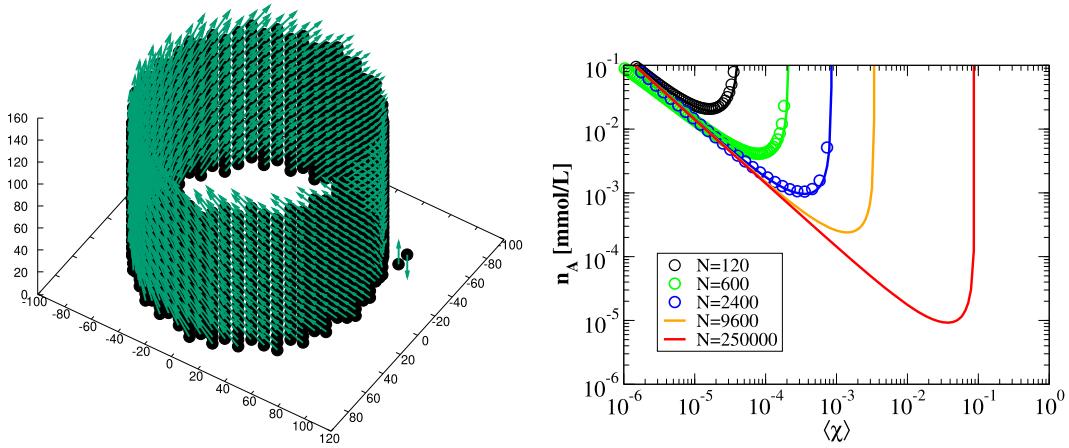

Figure 5. (a) Positions of the chromophores (circles) and transition dipole orientations (arrows) for the bio-mimetic complexes inspired to the GSB antenna complex considered in section 4.2. Axes are in Å units. Excitation energies, position, TDM orientation for this bio-mimetic aggregate are taken from references [33, 59, 60]. (b) Lasing threshold density under natural sunlight for a dimer coupled to a GSB nanotube. Symbols have been obtained by diagonalizing the whole aggregate Hamiltonian and using equation (8). Continuous curves have been obtained using the lasing equation, equation (8), for the dimer only with a modified pumping $R_u \to NR_u/2$, where N is the total number of chromophores in the aggregate composed of a nanotube and a dimer. System sizes up to $N = 250\,000$, corresponding to a realistic number of molecules in the whole GSB chlorosome [33, 59, 60], have been considered. However, as we discuss in the text, aggregate sizes $N \gtrapprox 4000$ stretch the validity of the assumptions of our laser equations, and are thus of indicative rather than literal value.

of a dimer alone whose R_u pumping factor is multiplied by $N/2$, where N is the total number of molecules in the whole aggregate (nanotube plus dimer).

As one can see, the effect of this different bio-inspired aggregate is similar to the purple bacteria molecular aggregate, which is to increase the pumping of the dimer by a factor $N/2$. The curves corresponding to the largest aggregates sizes ($N = 9600, 250\,000$) have been obtained only using the dimer equations with enhanced pumping. The results presented are very promising since they indicate the possibility to achieve lasing under natural sunlight for relatively large dimer brightness $\langle\chi\rangle \sim 10^{-1}$ (which is reachable experimentally [18]).

Notwithstanding the promising results in figure 5(b) for larger GSB aggregates, a word of caution is in order: as discussed in the following, applying our lasing equations to very large aggregates stretches the assumptions we have made in deriving equations (6)–(9) beyond its strict regime of validity. This renders quantitative conclusions unreliable, however, we believe the extrapolation can nonetheless give an indicative picture of the expected qualitative trend.

Specifically, we expect the implicit assumption that thermalization in the overall system Hamiltonian eigenbasis is the fastest timescale, to break for very large aggregates. On the one hand, it could be argued that disorder in large structures will lead to more localised states and the picture of completely delocalised eigenstates becomes questionable. On the other hand—and neglecting disorder for now—collective enhancements in the radiative rates will at some point change the hierarchy of timescales. To discuss this issue we now compare the fluorescence and the thermalization timescales: in large aggregates the dipole strength $|\mu_{\rm SR}/\mu|^2$ of the superradiant state in the nanotube scales with the number of molecules as $|\mu_{\rm SR}/\mu|^2 \approx 0.6N$ [33]. This means that the radiative decay time of the superradiant state is $\tau_{\rm fl} = \tau_0/|\mu_{\rm SR}/\mu|^2$, where $\tau_0 \approx 30$ ns is the radiative decay time of a single molecule. The overall thermalization timescale is given by the thermalization on the nanotube followed by the excitation transfer time from the nanotube to the dimer. Since the latter can be enhanced by lowering the distance between the dimer and the nanotube, we will solely focus on the nanotube thermalization time in the following. An upper bound for the thermalization timescale $\tau_{\rm th}$ can be obtained from the diffusion coefficient $D \approx 200$ nm^2 ps^{-1} as estimated for the GSB nanotubes in [61], through the relationship $\tau_{\rm th} = L^2/D$, where L is the length of the nanotube. For the natural nanotube considered here we have $L \approx N(0.01$ nm). The given estimates of thermalization and fluorescence times suggest that for a nanotube of $N \approx 4000$ molecules we obtain $\tau_{\rm th} \approx \tau_{\rm fl}$. We would therefore expect the laser equations derived in this manuscript to become quantitatively unreliable for $N \gtrapprox 4000$.

Adequately capturing the dynamics of larger aggregates with an explicit model is beyond the scope of the current work, and would require the derivation of lasing equations without the assumption of quasi-instantaneous vibrational thermalization, while keeping the large dephasing assumption inducing

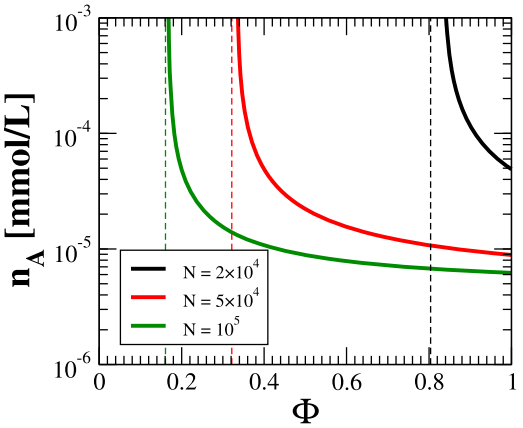

Figure 6. Threshold density, see equation (8), as a function of the emission quantum yield Φ, see equation (13), for a dimer under natural sunlight, with relative brightness $\langle\chi\rangle = 0.01$. Here we re-scale the absorption rate R_u by a factor $N/2$ to reproduce the effect of surrounding the dimer with an aggregate of $N-2$ molecules, as discussed in the text. Different values of N are considered, see figure. The vertical dashed lines represent the minimal quantum yield, see equation (14). Other parameters: $\hbar\omega_A = 1.17$ eV, $\Omega = 2000\ \mathrm{cm}^{-1}$, $\Gamma_\phi = 1/(10\ \mathrm{ps})$ and $\kappa/(2\pi) = 50$ MHz.

incoherent cavity driving. This means that one should use incoherent laser equations for these larger aggregates similar to equation (S60), used in the SM.

For the above reason, we only show circled data points for nanotubes up to $N = 2400$ in figure 5(b). Up to this point the required lasing dimer threshold brightness approaches 10^{-3}, and we note that this value is still almost an order of magnitude better than the best result shown in the previous subsection using the purple bacteria bio-inspired aggregate (cf figure 2(h)). However, we believe the solid extrapolation curves shown in figure 5(b) for larger N will nevertheless capture the trend for longer nanotubes, not least since much larger photosynthetic aggregates are known to be highly efficient at channelling energy excitations over long distances to the RCs. This extrapolation suggests that larger photosynthetic structures can indeed further significantly lower the lasing threshold requirements in terms of molecular density and dimer brightness.

5. Effects of nonradiative decay and quantum yield

Here we investigate the effects on nonradiative decay on the lasing threshold. As for BChla building blocks of the antenna systems, nonradiative decay gives an individual BChla excitonic lifetime of about 1 ns [6, 9], which is much longer than the time needed to transfer the excitation to the central dimer (of order tens of picoseconds [10, 11]). For this reason, when considering natural antenna complexes nonradiative effects can be safely neglected[12]. On the other hand, the effect of nonradiative decay on the H-dimer can be relevant, and we analyze it in more detail in the following.

Nonradiative decay can be included in our model as an additional decay channel in the dimer, with a decay rate γ_{nr}. In practice, this is equivalent to replacing $R_d \to R_d + \gamma_{\mathrm{nr}}$ in all our equations. We quantify the amount of nonradiative decay by means of the widely used emission quantum yield $\Phi = \gamma_{\mathrm{r}}/(\gamma_{\mathrm{r}} + \gamma_{\mathrm{nr}})$, where γ_{r} is the radiative decay rate. For an H-dimer, we have $\gamma_{\mathrm{r}} = \langle\chi\rangle\gamma_0$, see equation (9), so that we have:

$$\Phi = \frac{\langle\chi\rangle\gamma_0}{\langle\chi\rangle\gamma_0 + \gamma_{\mathrm{nr}}}, \tag{13}$$

where γ_0 is the radiative decay rate for each of the molecules composing the dimer.

A minimal quantum yield is necessary to obtain population inversion and, therefore lasing. In fact (see equation (6) and the following calculations) we reach population inversion only if $R_u > R_d$, but since the total decay rate is $R_d = \langle\chi\rangle\gamma_0 + \gamma_{\mathrm{nr}}$, using equation (13) we have the condition

$$\Phi > \frac{\langle\chi\rangle\gamma_0}{R_u}. \tag{14}$$

For natural sunlight and our choice of parameters for the dimer, we can approximate $R_u \approx 6.22\times10^{-7}N\gamma_0$, where N is the number of molecules in the aggregate, so that equation (14) becomes

[12] If we were to include them, they would only mildly reduce the effective pumping rate.

$\Phi > \langle\chi\rangle 10^7/(6.22N)$. Note also that $\Phi \leqslant 1$ by definition, so if the right-hand side of equation (14) is larger than unity, lasing is not possible.

In figure 6 the dependence of the threshold density n_A (continuous lines) on the quantum yield Φ is shown, under natural sunlight. Data in figure 6 have been obtained for a dimer brightness $\langle\chi\rangle = 0.01$, which is consistent with literature [19]. We increase the pumping by a factor $N/2$ to account for pumping by the surrounding aggregate, see discussion related to figures 3(h) and 5(b). As one can see from figure 6, the threshold density increases and diverges as the quantum yield approaches the minimal value from equation (14), see the dashed vertical lines. For these parameters, a large aggregate size $N > 10^4$ is required to meet the lasing threshold under natural sunlight. Indeed, as figure 6 shows, the minimal quantum yield is ≈ 0.8 for $N = 2 \times 10^4$, but it can be reduced to ≈ 0.3 by increasing N just by a factor of 2.5. These values of the quantum yield are realistic for several H-dimers reported in literature [19].

6. Conclusions and perspectives

Efficient sunlight-pumped lasers could revolutionize renewable energy technologies. Here we have shown how lasing with natural sunlight pumping can be achieved by mimicking the architecture of photosynthetic antenna complexes.

We first considered an ensemble of molecular H-dimers inside an optical cavity pumped by black-body cavity radiation. When considering realistic values of the H-dimer darkness, lasing is possible for high black-body temperatures which can be achieved by heating up a cavity with concentrated sunlight. Nevertheless, lasing with H-dimers under natural sunlight would require a very high level of darkness, which is very difficult to achieve. The main limitation is due to the very weak pumping produced by natural sunlight. Larger molecular H-aggregates might be able to lower the lasing threshold by absorbing more light and thus increasing the pumping. On the other hand, if not properly designed, large aggregates have an increased density of states which would suppress the thermal population of the lasing state. This effect would compete with the advantage gained by more absorbed light. In order to increase the absorbed light without suppressing the population of the lasing state, one possibility is to consider an aggregate which absorbs light on a hierarchy of energy scales and which is able to efficiently funnel the absorbed energy to a low energy lasing state which is well-gapped below other excitonic states. In this way, its thermal population will not be suppressed. These are precisely the features which characterize many natural antenna photosynthetic systems. Our proposed bio-inspired molecular aggregate serving as the lasing medium is composed of an H-dimer operating at low energy, surrounded by LHI and LHII rings of the purple bacteria antenna complex, which absorb at higher energy and efficiently funnel the absorbed energy to the H-dimer. In this configuration, we show that lasing should be possible even under natural sunlight illumination.

For a single-mode lasing cavity we can expect an output spectrum with properties similar to that of other organic die lasers, that is well approximated by a Lorentzian with a width determined by the cavity finesse. The specific bio-inspired parameters we have analysed would implement a short wavelength infrared laser, which has the advantage of being able to efficiently distribute converted solar energy due to the low dispersion in this wavelength range [53]. This is why this spectral regime is used in optical fiber communications. As an interesting prospect, our bio-mimetic molecular aggregates should be able to lase in nanocavities with volume of $(\lambda/20)^3$ [62] and could thus be engineered into sunlight-pumped nanolasers [63]. Indeed, we have shown that the required densities for achieving lasing under natural sunlight are about $n_A \approx 3\ \mu\text{mol l}^{-1}$, meaning about one dimer surrounded by a purple bacteria antenna composed of an LHI and 8 LHII (reaching a length of 15 nm) every 80 nm. This density is thus achievable in a single nanocavity. We also note that purple bacteria antenna complexes are naturally arranged on spherical shells, each about 70 nm in diameter and containing ≈ 30 RCs [6]. Thus in this spherical shell each RC is surrounded by about one/two hundreds of chlorophyll molecules, which is the same order of magnitude considered in this manuscript for the largest purple bacteria antenna complex analyzed (1 LHI and 8 LHII), see figure 3(e). If we replaced all the RCs with H-dimers, the volume of a single spherical shell would contain a dimer density of 0.3 mmol l^{-1}, that is 100 times higher than required for lasing, see figure 3(g). Therefore, placing such spherical shells in a cavity with a volumetric density of 1 part per 100, would still be enough to achieve lasing under natural sunlight illumination, provided that the H-dimers are dark enough.

Our idea can be generalized to other bio-inspired molecular architectures where molecular (J-)aggregates efficiently pump the bright state of a homo-dimer; this would allow lasing in other spectral regimes, and utilising other photosynthetic systems, e.g. the chlorosome of GSB [64] as already discussed here, or photosynthetic membranes such as in Photosystem II [65] to feed excitations into $|H\rangle$ and make them available for the lasing transition. Biomimetic antennae with controllable spacing between pigments [66] might offer further avenues for improving and tuning pumping efficiency. Even in its current form,

however, our proposed biomimetic architecture is sufficiently efficient at collecting light from weak sources that it holds the potential to serve as a spring-board architecture for other bio-mimetic quantum devices, including photon sensing, improved solar cells, or even quantum batteries.

Acknowledgments

We thank Alessia Valzelli for her help on the green sulfur bacteria antenna system. GLC and FM acknowledge Fausto Borgonovi for useful discussions. WMB thanks the EPSRC (Grant No. EP/L015110/1) for support. SO acknowledges the support from the MAECI project PGR06314-ENYGMA. EMG acknowledges support from the Royal Society of Edinburgh and Scottish Government and EPSRC Grant No. EP/T007214/1. GLC acknowledges the funding of ConaCyt Ciencia Basica project A1-S-22706. NP acknowledges the support by the European Union (EU) Horizon 2020 program in the framework of the European Training Network ColOpt, grant agreement 721465.

Data availability statement

All data that support the findings of this study are included within the article (and any supplementary files).

Author contributions

GLC and FM conceived the study. NP and SO developed the semi-classical laser theory. GLC and FM developed the incoherent laser equations and derived the laser equations presented in the main text. EG and WB developed the BR master equation and the coherent laser equations. FM and WB did most of the numerical simulations. EG and GLC directed the research. All authors contributed to writing of the manuscript.

ORCID iDs

Francesco Mattiotti https://orcid.org/0000-0002-2532-8876
Nicola Piovella https://orcid.org/0000-0003-2403-0776
Stefano Olivares https://orcid.org/0000-0002-9251-0731
Erik M Gauger https://orcid.org/0000-0003-1232-9885
G. Luca Celardo https://orcid.org/0000-0002-3679-1954

References

[1] Ritz T, Adem S and Schulten K 2000 *Biophys. J.* **78** 707–18
[2] Rodgers C T and Hore P J 2009 *Proc. Natl Acad. Sci.* **106** 353–60
[3] Gauger E M, Rieper E, Morton J J, Benjamin S C and Vedral V 2011 *Phys. Rev. Lett.* **106** 040503
[4] Hiscock H G, Worster S, Kattnig D R, Steers C, Jin Y, Manolopoulos D E, Mouritsen H and Hore P J 2016 *Proc. Natl Acad. Sci.* **113** 4634–9
[5] Strümpfer J, Sener M and Schulten K 2012 *J. Phys. Chem. Lett.* **3** 536–42
[6] Sener M K, Olsen J D, Hunter C N and Schulten K 2007 *Proc. Natl Acad. Sci.* **104** 15723–8
[7] Beatty J T, Overmann J, Lince M T, Manske A K, Lang A S, Blankenship R E, Van Dover C L, Martinson T A and Plumley F G 2005 *Proc. Natl Acad. Sci.* **102** 9306–10
[8] Baghbanzadeh S and Kassal I 2016 *J. Phys. Chem. Lett.* **7** 3804–11
[9] Baghbanzadeh S and Kassal I 2016 *Phys. Chem. Chem. Phys.* **18** 7459–67
[10] Hu X, Ritz T, Damjanović A and Schulten K 1997 *J. Phys. Chem.* B **101** 3854–71
[11] Hu X, Damjanovic A, Ritz T and Schulten K 1998 *Proc. Natl Acad. Sci.* **95** 5935–41
[12] Engel G S, Calhoun T R, Read E L, Ahn T-K, Mančal T, Cheng Y-C, Blankenship R E and Fleming G R 2007 *Nature* **446** 782–6
[13] Panitchayangkoon G, Hayes D, Fransted K A, Caram J R, Harel E, Wen J, Blankenship R E and Engel G S 2010 *Proc. Natl Acad. Sci.* **107** 12766–70
[14] Grad J, Hernandez G and Mukamel S 1988 *Phys. Rev.* A **37** 3835
[15] Spano F C and Mukamel S 1989 *J. Chem. Phys.* **91** 683–700
[16] Celardo G L, Borgonovi F, Merkli M, Tsifrinovich V I and Berman G P 2012 *J. Phys. Chem.* C **116** 22105–11
[17] Ferrari D, Celardo G L, Berman G P, Sayre R T and Borgonovi F 2014 *J. Phys. Chem.* C **118** 20–6
[18] Patlolla P R, Das Mahapatra A, Mallajosyula S S and Datta B 2018 *New J. Chem.* **42** 6727–34

[19] Caselli M, Latterini L and Ponterini G 2004 *Phys. Chem. Chem. Phys.* **6** 3857–63
[20] Gavrilenko V I and Noginov M A 2006 *J. Chem. Phys.* **124** 044301
[21] Hestand N J and Spano F C 2018 *Chem. Rev.* **118** 7069–163
[22] Scully M O 2010 *Phys. Rev. Lett.* **104** 207701
[23] Dorfman K E, Voronine D V, Mukamel S and Scully M O 2013 *Proc. Natl Acad. Sci.* **110** 2746–51
[24] Scully M O, Chapin K R, Dorfman K E, Kim M B and Svidzinsky A 2011 *Proc. Natl Acad. Sci.* **108** 15097–100
[25] Creatore C, Parker M A, Emmott S and Chin A W 2013 *Phys. Rev. Lett.* **111** 253601
[26] Fruchtman A, Gómez-Bombarelli R, Lovett B W and Gauger E M 2016 *Phys. Rev. Lett.* **117** 203603
[27] Higgins K, Benjamin S, Stace T, Milburn G, Lovett B W and Gauger E 2014 *Nat. Commun.* **5** 1–7
[28] Zhang Y, Oh S, Alharbi F H, Engel G S and Kais S 2015 *Phys. Chem. Chem. Phys.* **17** 5743–50
[29] Brown W M and Gauger E M 2019 *J. Phys. Chem. Lett.* **10** 4323–9
[30] Gierschner J, Varghese S and Park S Y 2016 *Adv. Opt. Mater.* **4** 348–64
[31] Özçelik S, Özçelik I and Akins D L 1998 *Appl. Phys. Lett.* **73** 1949–51
[32] Hindman J C, Kugel R, Wasielewski M R and Katz J J 1978 *Proc. Natl Acad. Sci.* **75** 2076–9
[33] Gullì M, Valzelli A, Mattiotti F, Angeli M, Borgonovi F and Celardo G L 2019 *New J. Phys.* **21** 013019
[34] Council N R 2014 *Advancing Land Change Modeling* (*Opportunities and Research Requirements*) (Washington, DC: The National Academies Press)
[35] Yabe T *et al* 2007 *Appl. Phys. Lett.* **90** 261120
[36] Uchida S *et al* 2006 Experimental study of solar pumped laser for magnesium-hydrogen energy cycle *AIP Conf. Proc.* **830** 439–46
[37] Graham-Rowe D 2010 *Nat. Photonics* **4** 64
[38] Reusswig P D, Nechayev S, Scherer J M, Hwang G W, Bawendi M G, Baldo M A and Rotschild C 2015 *Sci. Rep.* **5** 14758
[39] Masuda T, Iyoda M, Yasumatsu Y, Dottermusch S, Howard I A, Richards B S, Bisson J F and Endo M 2020 *Commun. Phys.* **3** 1–6
[40] Celardo G L, Angeli M, Craddock T J A and Kurian P 2019 *New J. Phys.* **21** 023005
[41] Chan H C H, Gamel O E, Fleming G R and Whaley K B 2018 *J. Phys. B: At. Mol. Opt. Phys.* **51** 054002
[42] Pachón L A, Botero J D and Brumer P 2017 *J. Phys. B: At. Mol. Opt. Phys.* **50** 184003
[43] De Mendoza A M, Caycedo-Soler F, Huelga S F and Plenio M B 2020 *New J. Phys.* **22** 073042
[44] Kassal I, Yuen-Zhou J and Rahimi-Keshari S 2013 *J. Phys. Chem. Lett.* **4** 362–7
[45] Chenu A, Brańczyk A M, Scholes G D and Sipe J E 2015 *Phys. Rev. Lett.* **114** 213601
[46] Shatokhin V N, Walschaers M, Schlawin F and Buchleitner A 2018 *New J. Phys.* **20** 113040
[47] Brumer P and Shapiro M 2012 *Proc. Natl Acad. Sci.* **109** 19575–8
[48] Olšina J, Dijkstra A G, Wang C and Cao J 2014 Can natural sunlight induce coherent exciton dynamics? (Preprint arXiv:1408.5385)
[49] Breuer H P and Petruccione F 2002 *The Theory of Open Quantum Systems* (Oxford: Oxford University Press)
[50] Zhang Y, Celardo G L, Borgonovi F and Kaplan L 2017 *Phys. Rev.* E **95** 022122
[51] Pavlopoulos T 2002 *Prog. Quantum Electron.* **26** 193–224
[52] Würfel P and Würfel U 2016 *Physics of Solar Cells* (*From Basic Principles to Advanced Concepts*) (New York: Wiley)
[53] Deshmukh A P, Koppel D, Chuang C, Cadena D M, Cao J and Caram J R 2019 *J. Phys. Chem.* C **123** 18702–10
[54] Scully M O and Zubairy M S 1999 *Quantum Optics* (Cambridge: Cambridge University Press)
[55] Zhu S Y, Scully M O, Fearn H and Narducci L M 1992 *Z. Phys.* D **22** 483–93
[56] Hu X and Schulten K 1998 *Biophys. J.* **75** 683–94
[57] Hu X, Ritz T, Damjanović A, Autenrieth F and Schulten K 2002 *Q. Rev. Biophys.* **35** 1–62
[58] Günther L M, Jendrny M, Bloemsma E A, Tank M, Oostergetel G T, Bryant D A, Knoester J and Köhler J 2016 *J. Phys. Chem* B **120** 5367–76
[59] Sawaya N P D, Huh J, Fujita T, Saikin S K and Aspuru-Guzik A 2015 *Nano Lett.* **15** 1722–9
[60] Linnanto J M and Korppi-Tommola J E I 2013 *J. Phys. Chem.* B **117** 11144–61
[61] Fujita T, Brookes J C, Saikin S K and Aspuru-Guzik A 2012 *J. Phys. Chem. Lett.* **3** 2357–61
[62] Yao J, Yang X, Yin X, Bartal G and Zhang X 2011 *Proc. Natl Acad. Sci.* **108** 11327–31
[63] Ma R-M and Oulton R F 2019 *Nat. Nanotechnol.* **14** 12–22
[64] Huh J, Saikin S K, Brookes J C, Valleau S, Fujita T and Aspuru-Guzik A 2014 *J. Am. Chem. Soc.* **136** 2048–57
[65] Amarnath K, Bennett D I G, Schneider A R and Fleming G R 2016 *Proc. Natl Acad. Sci.* **113** 1156–61
[66] Lindsey J S 2015 *Chem. Rev.* **115** 6534–620